Prediction of temperature-dependent nucleation and growth rates from crystallization-related heat release

Joseph Kangas ●* and Christopher J. Hogan, Jr. ●†

Department of Mechanical Engineering, University of Minnesota. 111 Church St SE, Minneapolis MN 55455, USA

We propose a method for determining the time and, therefore, temperature-dependent relative nucleation and growth rates during crystallization. We do so by linking the partial differential equation governing the time dynamics of the crystal size distribution to kinetic (Avrami) parameters describing heat release. This approach is tested *in silico* by nucleating and growing diffusion limited aggregates with time-varying morphology and growth rates unhindered by impingement. The associated heat release is analyzed, showing that nucleation and growth rates could be extracted with high fidelity.

I. INTRODUCTION

Nucleation, involving the formation of growing regions of a new phase from a parent phase, is one of the most fundamental phenomena in physics and chemistry. Characterization of these first-order phase transitions, especially the nucleation and growth time dynamics, is important for understanding a diversity of topics throughout the physical and biological sciences, from defect growth in amorphous silica to the formation of ice crystals in cells [1,2]. A common challenge in the investigation of phase change time dynamics is that the spatiotemporal resolution of current direct measurement techniques for liquid-solid nucleation rates is lacking in the majority of systems at most temperatures, especially those in 'no man's' land below the homogeneous nucleation temperature [3–6]. Existing methods rely on direct optical observation of nuclei formation, requiring tight constraints on system opacity and both the temporal and spatial scale over which nucleation occurs. Instead, a variety of indirect methods are commonly deployed to measure macroscopic system properties during phase change, ultimately linking these to nucleation and growth via a variety of thermodynamic and kinetic models, including classical nucleation theory. Such techniques include measurements of induction times and metastable zone widths [7,8]; transformed fraction measurements via Fourier transform infrared spectroscopy [9], differential scanning calorimetry (DSC) [10–12], and differential thermal analysis [13]; and crystal size distribution measurements via laser [14] and x-ray diffraction [15], which suffer from calibration difficulties, poor temporal resolution, and measurement difficulties in liquids systems. Unfortunately, indirect methods for measuring nucleation rates often suffer from the same fatal flaw, i.e., reliance on empirically determined kinetic parameters such as activation energy or fitting parameters without theoretical justification, and no clear method of comparing the model results to either real

or simulated nucleation or growth measurements [16,17]. It is then not surprising that even for water, one of the most well-characterized substances, nucleation rate measurements for the same temperatures may vary by over four orders of magnitude [18].

In this paper, we derive an approach to determine nucleation and growth rates more directly, with minimal assumptions. To do so, we consider DSC, which is arguably the most simple of the aforementioned measurement techniques to employ. In DSC, the latent heat released during phase change is measured, which can be related to the fraction of a newly formed phase in the system, given knowledge of the heat of fusion of said phase. This transformed fraction $f(t)$ can be determined by integrating the baseline corrected heat flow per unit mass $q(t)$ between the onset and offset times of solidification and then dividing by the enthalpy of fusion $\Delta H_{\text{fus}}^{\circ}$ [19]:

$$\dot{f}(t) = \frac{q(t)}{\Delta H_{\text{fus}}^{\circ}(T)}. \qquad (1)$$

The transformed fraction has long been shown, under isothermal conditions, to follow the Avrami equation, also known as Johnson-Mehl-Avrami-Kolmogorov (JMAK) equation [20–22], expressed as

$$f(t) = 1 - \exp(-kt^n), \qquad (2)$$

where k is a kinetic parameter relating to the nucleation and growth of the new phase while n is related to the morphology, which can both be determined via least-squares regression [23–26]. Under idealized conditions, when the growing nuclei morphology is easily expressible, such as a sphere, rod, or disk, k and n can be derived from first principles; however, a cohesive theory deriving the Avrami equation for general arbitrary morphological growth has yet to be demonstrated until now, which we show provides an avenue for extracting three key fundamental parameters of phase change from latent heat release curves. These three key fundamental parameters are the nucleation rate J, growth rate u, and fractal dimension D of the newly formed phase, describing the rate of formation of new phase nuclei (number per unit time per

unit volume), their growth rate (length per unit time), and morphology (nondimensional), respectively. Throughout this paper, we will demonstrate under what conditions the Avrami equation remains valid; how k and n are related to the fundamental parameters J, u, and D; and how these fundamental parameters can be extracted from heat release curves. We will refer specifically to crystallization, but the arguments presented hold equally true for many other phase change processes. As in the original formulation of JMAK kinetics, we treat growing regions of the phase independently, that is, they pass through each other without alteration of the growth or nucleation mechanics. Though this seems at first nonphysical, it is merely a mathematical trick which transforms an extremely complex problem involving overlapping geometries into a relatively simple one solvable with standard calculus. Though this treatment may break down under certain circumstances, the success of the JMAK equation in describing phase change in many systems shows it to be a valid assumption.

II. LINKING THE AVRAMI PARAMETERS TO CRYSTAL NUCLEATION AND GROWTH RATES

We start by considering a crystal with an arbitrary morphology. The volume V of this crystal can be described in terms of some length scale L, dimensionality D, and density-volume scaling parameter A:

$$V = AL^D. \tag{3}$$

We now consider a spherical-equivalent crystal, referred to as the packed-volume crystal, with radius r and volume equal to that of the arbitrary morphology crystal in Eq. (3). Relating the volumes of these two crystals yields

$$AL^D = \frac{4\pi}{3} r^3. \tag{4}$$

Next, by differentiating Eq. (4) with respect to time, we determine how the growth rate of the characteristic length L relates to the radius of the packed-volume crystal:

$$\frac{dL}{dt} = \frac{3}{D} \left(\frac{4\pi}{3A} \right)^{\frac{1}{D}} r^{\frac{3}{D}-1} \frac{dr}{dt}. \tag{5}$$

Under conditions of constant growth, the crystal with arbitrary morphology grows at a velocity v_0, which can be related to the growth rate of the packed-volume crystal $u(r)$ via the packed-volume scaling factor α,

$$\alpha = \frac{3}{D} \left(\frac{4\pi}{3A} \right)^{\frac{1}{D}}, \tag{6}$$

$$\frac{dr}{dt} = u(r), \quad \frac{dL}{dt} = v_0, \quad v = v_0/\alpha, \quad m = \frac{3}{D} - 1, \tag{7}$$

$$u(r) = \frac{v}{r^m}, \tag{8}$$

where m is related to the fractal dimension D of the growing arbitrary morphology crystal and v is the morphology-scaled growth rate. By definition, the packed-volume crystal is perfectly volume filling, so its growth rate will decay with its increasing radius, as the length scale of the arbitrary morphology crystal increases at a constant velocity. It becomes mathematically convenient to use the packed-volume velocity

when describing the time dynamics of the crystal size distribution $\rho(r, t)$, which defines the number of packed-volume crystals of radii r per unit volume per unit radii. The time evolution of $\rho(r, t)$ is described by the population balance equation, given an initial crystal size distribution $R_0(r)$, nucleation rate $J(t)$, and packed-volume growth rate $u(r, t)$ [27,28]:

$$\frac{\partial \rho(r, t)}{\partial t} + \frac{\partial}{\partial r}(u(r, t)\rho(r, t)) = 0,$$

$$\rho(r, 0) = R_0(r),$$

$$\rho(0, t) = \frac{J(t)}{u(0, t)}. \tag{9}$$

Previously, we presented a general solution to Eq. (9) when the growth rate and nucleation rate are time independent (i.e., under isothermal conditions), absent an initial distribution of transformed phase [29],

$$\rho(r, t) = \frac{J}{u(r)} \theta \left(t - \int_0^r \frac{dy}{u(y)} \right), \tag{10}$$

where θ is the Heaviside step function. The transformed fraction can be related to the crystal size distribution by accounting for overlapping regions of phase via impingement correction [30]:

$$-\ln(1 - f(t)) = \int_0^\infty \frac{4\pi r^3}{3} \rho(r, t)\, dr. \tag{11}$$

By linking Eq. (11) to the Avrami equation and the solution described by Eq. (10), we can relate the Avrami coefficients k and n to the nucleation rate, morphology-scaled growth rate, and fractal dimension of the crystals, a detailed outline of which is given in Appendix A:

$$k = \frac{4\pi(1+m)}{3(4+m)} J((m+1)v)^{\frac{3}{m+1}} = \frac{4\pi J}{3(D+1)} \left(\frac{3v}{D} \right)^D, \tag{12}$$

$$n = \frac{4+m}{1+m} = D + 1. \tag{13}$$

We will demonstrate the utility of Eqs. (12) and (13) by describing a method by which the temperature-dependent changes in crystal growth and nucleation rate can be extracted from heat-release (calorimetry) curves.

III. SOLID-PHASE GROWTH AND NUCLEATION RATES FROM CALORIMETRIC CURVES

A. Extracting the Avrami parameters k and n

Beyond providing insight into how crystal geometry influence the Avrami equation, the utility of Eqs. (12) and (13) is apparent in the analysis of calorimetric data, as extracting the Avrami parameters from a calorimetry curve is a well-established experimental method [19]. The transformed fraction $f(t)$ can be determined by integrating the baseline corrected heat flow per unit mass $q(t)$, equation (1), between the onset and offset times of solidification and then dividing by the enthalpy of fusion $\Delta H_{\mathrm{fus}}^{\circ}$. Then, k and n can be determined via linear fitting of the Avrami equation:

$$\ln(-\ln(1 - f(t))) = \ln(k) + n \ln(t). \tag{14}$$

Beyond the direct link to parameters defining nucleation and growth in Eqs. (12) and (13), we now show that modi-

fied calorimetry operation, specifically by introducing a step change in temperature during measurement, can be employed to directly determine relative change in nucleation and growth rates, as well as structural changes to growing nuclei for systems at different temperatures.

B. Calculating the change in nucleation and growth rates resulting from a step-change in temperature

First, we consider a system in the liquid state that is rapidly brought to a temperature T_1, below its melting point, and thus begins to solidify. Then, at time $t = s$, the system is rapidly brought to a second temperature T_2, also below the melting point. We assume the temperature transitions are fast compared to the rate of phase change, and thus phase change during the near-discontinuous temperature jumps can be neglected. Examining the changes in $\rho(r, t)$ across the temperature jump holds the key to extracting useful information about nucleation and growth in the system.

Via the method of characteristics, the solution to Eq. (9) has the form $\rho(r, t) = r^m g(r^{m+1} - (m + 1)vt)$ for some function g. Applying the initial and boundary conditions, along with the growth rate from Eq. (8), we arrive at

$$
\rho(r, t) = \theta\left(vt - \frac{r^{m+1}}{m + 1}\right)\frac{J}{v} + \theta(r^{m+1} - (m + 1)vt)
$$
$$
\times \frac{r^m R_0((r^{m+1} - (m + 1)vt)^{\frac{1}{m+1}})}{(r^{m+1} - (m + 1)vt)^{\frac{m}{m+1}}}. \tag{15}
$$

We then consider Eq. (8) at two different temperatures T_1 and T_2, then employ Eq. (15) to evaluate the system behavior as a consequence of the temperature jump at time $t = s$. For the T_1 case, there is no initial crystallization and the solution is

$$
\rho_1(r, t) = \theta\left(v_1 t - \frac{r^{m_1+1}}{m_1 + 1}\right)\frac{J_1}{v_1}r^{m_1}. \tag{16}
$$

Next, $\rho_1(r, s) = R_0(r)$ is used as the initial condition for the T_2 case, with the new time $t - s$. Since we are only concerned with the solution for small times after the temperature jump, we can ignore the term corresponding to the nucleation of new material:

$$
\rho_2(r, t) = \frac{J_1}{v_1}r^{m_2}\theta(r^{m_2+1} - (m_2 + 1)v_2(t - s))
$$
$$
\times \theta\left(v_1 s - \frac{(r^{m_2+1} - (m_2 + 1)v_2(t - s))^{\frac{m_1+1}{m_2+1}}}{m_1 + 1}\right)
$$
$$
\times (r^{m_2+1} - (m_2 + 1)v_2(t - s))^{\frac{m_1-m_2}{m_2+1}}. \tag{17}
$$

Examining the ratio of the time derivatives of the transformed fractions associated with $\rho_1(r, t)$ and $\rho_2(r, t)$ at time $t = s$, $\dot{f}_1(s)$ and $\dot{f}_2(s)$ respectively, we derive a link between this measurable ratio and the morphology-scaled growth rates:

$$
\frac{\dot{f}_2(s)}{\dot{f}_1(s)} = \beta\frac{v_2}{v_1^M}, \tag{18}
$$

where

$$
\beta = \left(\frac{3}{3 + m_1 - m_2}\right)(s(m_1 + 1))^{\frac{m_1 - m_2}{m_1 + 1}} \tag{19}
$$

$$
M = \frac{m_2 + 1}{m_1 + 1}. \tag{20}
$$

Using Eq. (1), we can now represent $\dot{f}_2(s)/\dot{f}_1(s)$ in terms of the heat flow and heat of fusion at temperature T_1, just before the temperature jump [$q_1(s)$ and $\Delta H_{\text{fus}}^{\circ}(T_1)$] and the heat flow and heat of fusion at temperature T_2, just after the temperature jump [$q_2(s)$ and $\Delta H_{\text{fus}}^{\circ}(T_2)$]:

$$
v_2 = \frac{v_1^M q_2(s)\Delta H_{fus}^{\circ}(T_1)}{\beta q_1(s)\Delta H_{fus}^{\circ}(T_2)}. \tag{21}
$$

Continuing in this fashion from T_2 to T_3, or even T_1 to T_3, we can infer $v(T_i)$ in terms of $v(T_1)$. Finally, from Eq. (12), the nucleation rate $J(T)$ can be determined in terms of $k(T)$, $v(T)$, and $n(T)$:

$$
J(T) = \frac{3k(T)n(T)}{4\pi}\left[\frac{3v(T)}{n(T) - 1}\right]^{1-n(T)}. \tag{22}
$$

We provide an the extension of this approach in two dimensions in Appendix B, which is applicable to phase change on surfaces, and used here in subsequent numerical experiments. Additionally, Appendix B includes a detailed derivation of Eq. (18). It is important to note that the nucleation rate J and the growth rate v_0 describe the supercooled portion of the system alone, denoted by $1 - f$. If one was interested in the systemwide nucleation rate, it would simply be $J_{\text{sys}} = (1 - f)J$.

C. Method for extracting the relative (or nonrelative) growth and nucleation rates

We desire to know the temperature-dependent growth and nucleation rates for a substance in some temperature interval $[T_0, T_f]$. To infer this from measurements, we first partition this interval into N temperature points $T_1, T_2, ..., T_N$. Next, for each temperature, we start the DSC run at some initial temperature above the melting temperature of the substance. From this temperature, we rapidly (as fast as possible) decrease the temperature to T_1 and hold it until the substance solidifies and reaches equilibrium. This isothermal curve can be analyzed to calculate n_1 and k_1 for T_1. The time s_1 when half of the available sample solidifies is also identified; this often corresponds to the peak location for the heat release $q_1(t)$. This procedure is then repeated for T_2 through T_N. Subsequently, a series of jumps between these temperature points need to be carried out, as depicted in Fig. 1. For the first jump, the sample is held at T_1 just as in the first trial, but for s_1 seconds, followed by a rapid change in the temperature to T_2. This approach continues with a sample starting at T_2 transitioned to T_3 and so on all the way through a sample starting at T_{N-1} transitioned to T_N. Using the curves $q_i(t)$ generated from the DSC trials (for the temperature jump from T_i to T_{i+1}), Eqs. (21) and (22) are then applied to obtain $v(T)$ and $J(T)$ in terms of $v(T_1)$. These temperature-dependent velocities and nucleation rates can then be normalized to $v(T_1)$ and $J(T_i)$. If desired, one can measure the velocity $u(T_1)$ of a single growing crystal
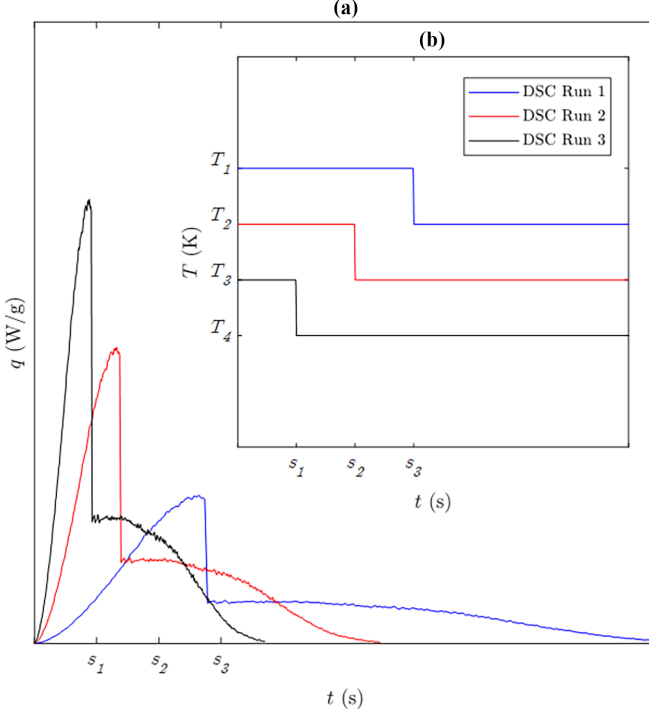
FIG. 1. Example heat-release curves (a) and associated temperature profiles (b) for the DSC protocol required for calculating the temperature-dependent changes in the nucleation and growth rate of the growing phase.

at T_1 (or one of the other temperature points), then, using its radius R and fractal dimension D (measured from DSC), can solve for $v(T_i)$, and thus know the temperature-dependent velocities and temperature-dependent nucleation rates in the temperature range from T_1 to T_N.

Although this approach follows directly from the solution to the differential equation governing nuclei growth, testing this procedure is experimentally difficult, as at present, we are not aware of a system where $v(T)$, $J(T)$, $n(T)$, and $k(T)$ are adequately established. Therefore, to examine the capabilities of this approach, we apply crystal growth simulations, simulating DSC curves for fractal-like structures whose fractal dimension of growth changes with system temperature.

IV. TIME-DEPENDENT DIFFUSION LIMITED AGGREGATION

We perform *in silico* experiments to extract the nucleation and growth rates from heat release curves via Eqs. (21) and (22) as, in this way, all nucleation and growth parameters can be known exactly *a priori*. We specifically simulate the growth of a system of two-dimensional pseudocrystals with predefined nucleation and growth rates via a time-dependent diffusion limited aggregation (TD-DLA) algorithm based on the classic algorithm and its more computationally efficient derivatives, as depicted schematically in Fig. 2(a) [31,32]. Additional details on this algorithm are provided in Appendix C. Briefly, using a two-dimensional grid, a series of TD-DLA structures are generated, which grow by a specified number of particles at each simulation time step. The growth rate is
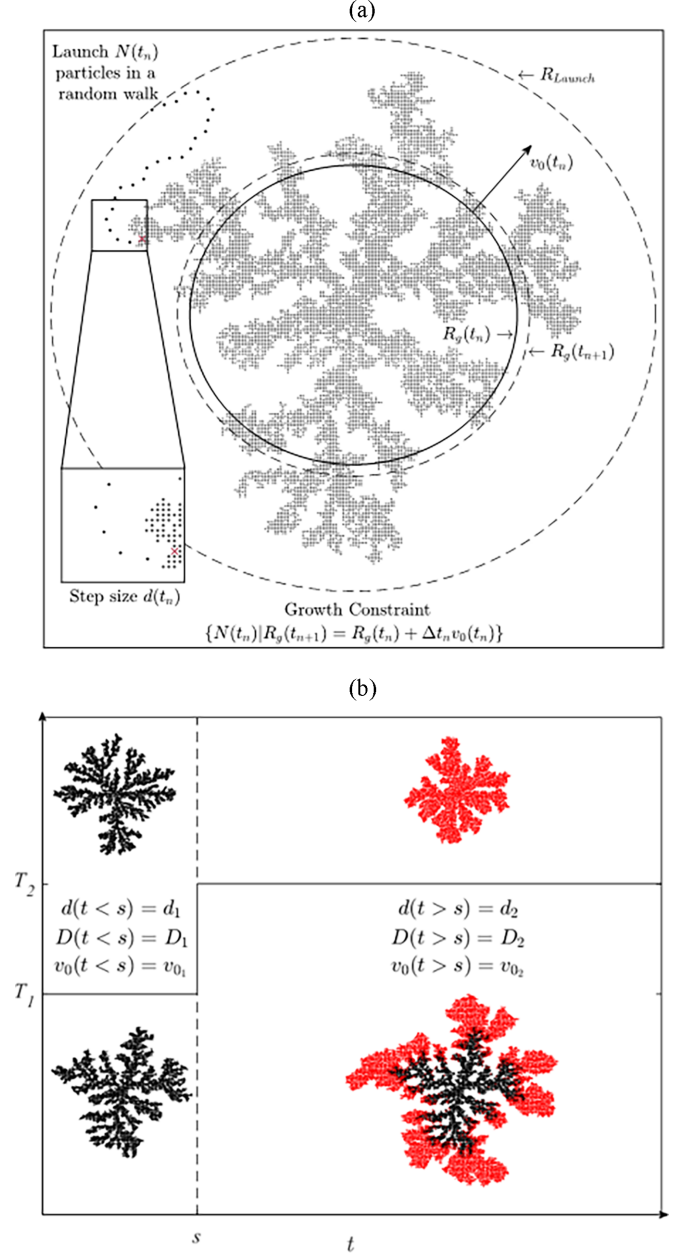

FIG. 2. (a) A schematic depiction of how time dependence is applied to a growing diffusion-limited aggregate in two dimensions. The applied algorithm allows for the tuning of fractal dimension by altering the step size $d(t_n)$ (or stickiness) and growth rate $v_0(t_n)$ by applying a growth constraint, growing the aggregate by $N(t_n)$ particles and increasing the radius of gyration $R_g(t_n)$ by $dt_n v_0(t_n)$. (b) The temperature-time profile for the simulation involving a step change from temperature T_1 to T_2 at time $t = s$, resulting in a step change in both growth rates $v_0(t)$ and step size $d(t)$ [and thus fractal dimension $D(t)$]. The temperature time profile and a simulated diffusion limited aggregate before (in black) and after (in red) the temperature jump are displayed. Also depicted is an aggregate nucleated before time s which contains the growth from before and after time s.

maintained by adhering to the growth constraint:

$$\{N(t_n)|R_g(t_{n+1}) = R_g(t_n) + \Delta t_n v_0(t_n)\}. \qquad (23)$$

For each generated aggregate, the number of particles added at time step t_n increases the radius of gyration $R_g(t_n)$ by $v_0(t_n)\Delta t_n$, such that the aggregate is now composed of $N(t_n)$ particles. The fractal dimension D is modulated by altering the random walk step size d or stickiness parameter, allowing for values of D between 1.71 and 2.0 in the continuous limit, see Fig. 2(b).

In growth simulations, the aggregates are seeded randomly on a grid and grow at a constant rate of $v_0(t_n)$, with their introduction rate following a nucleation rate $J(t_n)$ and time step Δt_n. The base unit added during nucleation is a monomer; we remark that the "critical size" defining the smallest stable nuclei does not influence the system as $J(t)$ and $u(t)$ are predefined in simulations, and our goal is strictly to use simulations to test Eqs. (21) and (22). Nucleation and growth are hence simulated in irreversible fashion, i.e., in a situation where the system is cooled well below its melting temperature. By construction, with fixed $J(t)$ and $u(t)$ in these simulations, the equation is valid to describe the fraction of transformed phase. For each new particle added to a growing aggregate, heat is released according to a prescribed heat of fusion $\Delta H_{\text{fus}}^{\circ}(t_n)$ at the simulation time (temperature). Intersection between pseudocrystals is ignored (i.e., not counted as a new phase, with no heat release) with periodic boundary conditions applied. Testing the validity and applicability of Eqs. (21) and (22) requires us to simulate the growth of TD-DLA pseudocrystals under conditions emulating a step change in temperature. To accomplish this, we predefine the system parameters at two temperatures, T_1 and T_2, with associated temperature-dependent growth rates u_1 and u_2 (thus v_1 and v_2), nucleation rates J_1 and J_2, fractal dimensions D_1 and D_2, and heat of fusions $\Delta H_{\text{fus},1}^{\circ}$ and $\Delta H_{\text{fus},2}^{\circ}$.

In this simulation, 875 diffusion limited aggregates were grown, consisting of between 1 and 50 000 particles depending on when they were nucleated during the simulation time span. A step size of 5 and 15 grid spaces were chosen for simulation temperatures T_1 and T_2, respectively, both with a stickiness value of 1.0. This allowed for distinguishable fractal growth between the two temperatures while allowing the aggregates to remain spatially dense to limit computational time. Due to these generation properties, each aggregate had a unique fractal dimension and geometry, with those formed at the same temperature having similar geometric properties, see Tables I and II. Growing nuclei did not interact with each other, as they represent individual crystals in the extended volume (total crystal volume disregarding overlap), an important quantity in Avrami kinetics. We simulate crystallization in this system under isothermal conditions at T_1 and T_2, as well as a step change in temperature $T_s(t)$ from T_1 to T_2 at time $t = s$. A comparison between theoretical prediction for the transformed fraction and those simulated under isothermal conditions is provided in Fig. 3(b). The strong agreement ($R^2 > 0.99$) between predictions and the simulations supports application of Eqs. (12) and (13) for crystals with complex morphologies with nonuniform dimensionality, given the size dependence of fractal dimension in diffusion limited aggregates. For the temperature jump condition, the time $t = s$ is chosen when half the system transformed phases so the newly nucleated phase is insignificant relative to the growing pre-existing phase. Additionally, the strongest heat release signal

TABLE I. The extracted Avrami parameters k and n, heat flow $q(s)$ immediately before and after the temperature jump, the heat of fusion $\Delta H_{\text{fus}}^{\circ}$, and bulk density-volume scaling parameter $\overline{A}$, and bulk packed-volume scaling factor $\overline{\alpha}$ at T_1 and T_2. The uncertainty shown represents 95% confidence bounds on the parameters from regression. The values of the parameters are given in dimensionless units.

Parameters	T_1	T_2
k	31.249 ± 0.220	6.424 ± 0.026
n	2.743 ± 0.005	2.938 ± 0.004
$q(s)$	3.868	1.262
$\Delta H_{\text{fus}}^{\circ}$	1	1.1
$\overline{A}$	8.07	6.89
$\overline{\alpha}$	0.668	0.688

often occurs near the moment the system is half transformed, i.e., $f(t) = 0.5$. In practice, this point would need to be determined by a first measurement where the phase change is monitored, holding the system at temperature T_1. Figure 2(b) depicts the change in aggregate morphology before and after the temperature jump, denoting crystal formation at T_1 in black and T_2 in red. The heat release curves resulting from isothermal temperature holds at T_1 and T_2, Fig. 3(a), are integrated to solve for the transformed fraction, Fig. 3(b), which enables extraction of the Avrami parameters k and n via equation (14) via curve fitting. Analyzing the resulting heat release curves associated with the step change in temperature via regression yields the parameters summarized in Table I. We extracted nearly identical growth rates and nucleation rates to those used as inputs in the simulation, as evidenced in Table II. This is true even though the crystals have a distribution of fractal dimensions, as is the case here due to the size dependence of fractal dimension in diffusion-limited aggregates. It is important to note again that the values of the calculated nucleation and growth rates are in terms of v_1, which means we have determined the relative change in these values, but not their absolute values. To determine the absolute values, one needs a single additional data point, v_1 or J_1 suffice, to determine the values of these parameters at all temperatures T_1 to T_i. Figures 3(c) and 3(d) depict snapshots of the crystallization simulation before ($t = .1$) and after ($t = .35$) the temperature jump ($s = .25$).

TABLE II. Values of the input versus extracted growth rates v_0, mean morphology-scaled growth rates $\overline{v}$, nucleation rates J, and mean fractal dimensions $\overline{D}$ at temperatures T_1 and T_2. The values of the parameters are given in dimensionless units. †Indicates a measured value for v_1, as one measurement is required to anchor all other nucleation and growth rate data. Without this value, one can normalize all other rates in terms of $\overline{v}_1$ or v_{0_1} to obtain the normalized growth and nucleation rate curves.

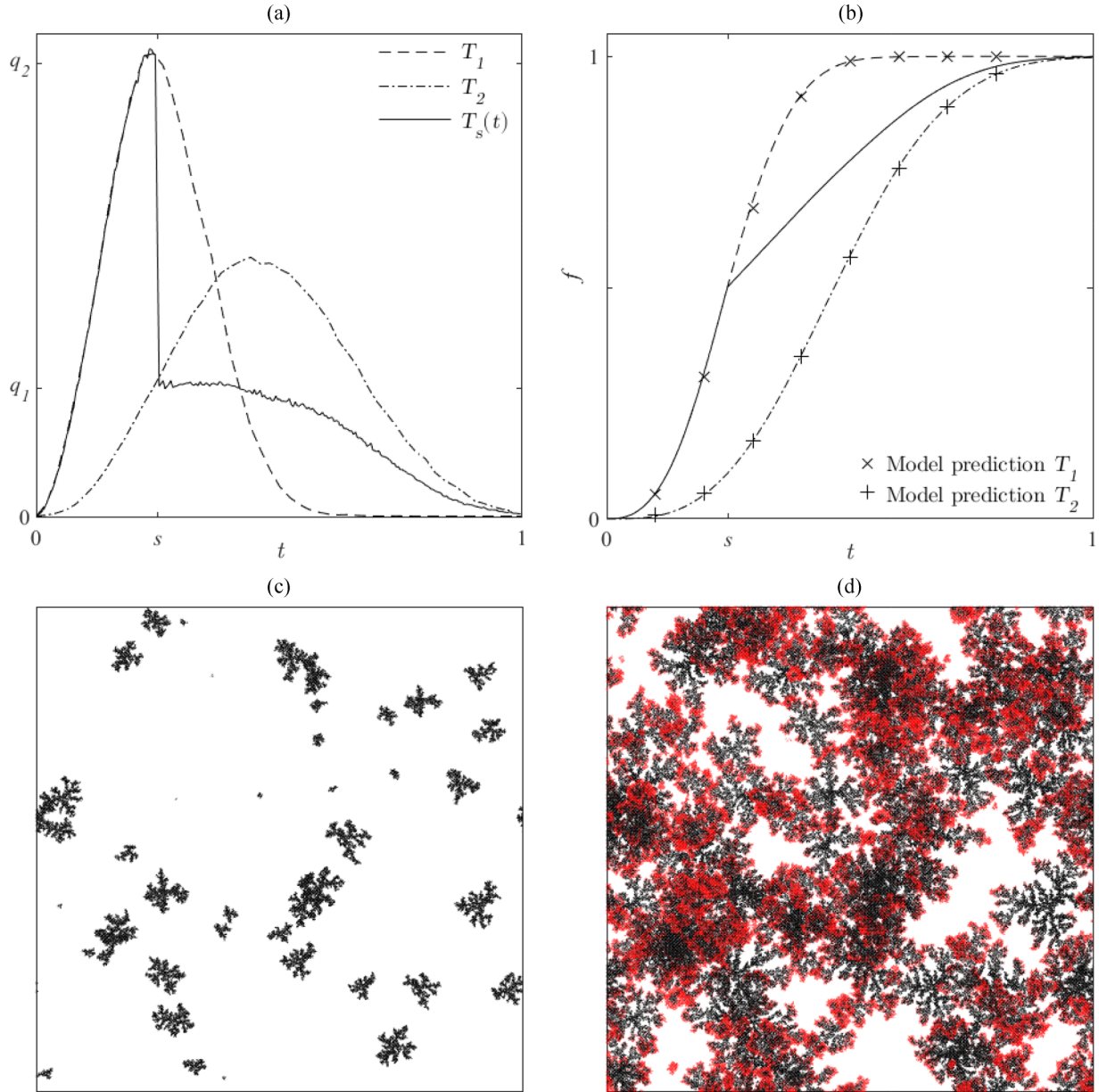| Parameters	T_1	T_1(predicted)	T_2	T_2(predicted)
v_0	300	$300^{\dagger}$	60	59.48
$\overline{v}$	449.21	$449.21^{\dagger}$	86.43	87.19
J	5×10^{-5}	5.11×10^{-5}	1×10^{-4}	9.97×10^{-5}
$\overline{D}$	1.757	1.743	1.904	1.938

FIG. 3. (a) The heat release q measured from crystal simulations resulting from isothermal holds at T_1 and T_2, as well as the temperature jump $T_s(t)$ from T_1 to T_2 at time $t = s$, with q_1 and q_2 referring to the heat release values before and after the temperature jump, respectively, in $T_s(t)$. These heat release curves can be integrated via Eq. (1) to calculate the transformed fraction for the three temperature cases, depicted in (b). The transformed fraction curves associated with isothermal crystallization simulation at temperatures T_1 and T_2 are shown along with the associated theoretical predictions ($\times$ and $+$, respectively) for these curves based on Eqs. (12) and (13), both of which have R^2 values of over 0.99. Additionally, the transformed fraction for $T_s(t)$ is also shown. Snapshots of the crystallization simulation at (c) $t = 0.1$ and (d) $t = 0.35$ with the temperature jump at $s = 0.25$. Crystallization before the temperature jump is depicted in black while crystallization after the temperature jump is depicted in red, illustrating the changing crystal morphology.

V. CONCLUSION

We utilize a population balance approach to model the heat release of a system undergoing first-order phase change involving nucleation and growth. In doing so, we show that the kinetic parameters extracted from the traditional Avrami equation k and n are functionally dependent upon the nucleation rate, growth rate, and growth geometry, here characterized by the fractal dimension. The exact solutions to our governing equations provide insight into performing calorimetry experiments, in which relative growth rates and nucleation rates, as well as growth geometries, can be extracted from calorimetric curves. The applicability of this approach, utilizing measurements of heat-release surrounding temperature jumps, is demonstrated through simulating diffusion-limited aggregates nucleating and growing in a periodic system. After testing the theory on simulated TD-DLA crystals, we have confidence that implementation of these methods for extracting relative changes in growth rates and nucleation rates from a system undergoing liquid-solid phase change will quantitatively yield the true changes in growth rates, nucle-

ation rates, and morphologies in that system relative to some baseline. Absolute values of the nucleation and growth rates only require the addition of one anchoring measurement, such as a growth rate measurement via microscopy. The method outlined in this paper is only contingent on the accuracy of the heat-release measurements, and that the DSC instrument can achieve changes in temperature sufficiently faster than the phase change at hand.

APPENDIX A: AVRAMI COEFFICIENTS

1. Derivation of Avrami constants

The Avrami equation can be rearranged as follows:

$$-\ln(1 - f(t)) = kt^n. \tag{A1}$$

Given Eqs. (10) and (11), and equating them to Eq. (A1), we have

$$kt^n = \int_0^\infty \frac{4\pi J r^{3+m}}{3v} \theta\left(t - \frac{r^{m+1}}{(m+1)v}\right) dr. \tag{A2}$$

For isothermal conditions, we have $u(r)$ described by Eq. (8), and for brevity we will now refer to $v(T)$ and $m(T)$ as simply v and m. By applying the following substitutions $z = \frac{r^{m+1}}{(m+1)v}$ and $dz = dr\frac{r^m}{v}$, we arrive at

$$kt^n = \frac{4\pi}{3} J((m+1)v)^{\frac{3}{m+1}} \int_0^\infty z^{\frac{3}{m+1}} \theta(t - z) dz, \tag{A3}$$

$$kt^n = \frac{4\pi(1+m)}{3(4+m)} J((m+1)v)^{\frac{3}{m+1}} t^{\frac{4+m}{1+m}}. \tag{A4}$$

This solution can conveniently be separated into two parts: a time-independent portion corresponding to k and an time-exponential portion corresponding to t^n. Equation (A4) thus yields

$$k = \frac{4\pi(1+m)}{3(4+m)} J((m+1)v)^{\frac{3}{m+1}} = \frac{4\pi J}{3(D+1)}\left(\frac{3v}{D}\right)^D. \tag{A5}$$

$$n = \frac{4+m}{1+m} = D + 1. \tag{A6}$$

2. Example of calculating parameters for a disk

For simple geometries, some solutions for n and k in terms of the fundamental parameters are known and summarized in Table III. As an additional example, we can consider the case where the growing solid is a disk of radius r. Since our model assumes dampened spherical growth instead of specific geometries, we can compare the relative radius of a sphere R vs disk r of equal volume:

$$\frac{4}{3}\pi R^3 = \pi r^2 D, \tag{A7}$$

$$r = \sqrt{\frac{4R^3}{3D}}. \tag{A8}$$

TABLE III. Equivalent values for the fractal dimension of the growing solid D_{f3D}, the radial growth parameter m, and the Avrami parameter n

$D_{f3\text{D}} =$	m	n
3 (spherically symmetric growth)	0	4
2 (circular symmetric growth)	.5	3
1 (linear symmetric growth)	2	2

Now comparing the velocity, the sphere grows in comparison to the disk:

$$\frac{dr}{dt} = \frac{dR}{dt}\sqrt{\frac{3R}{D}}. \tag{A9}$$

We denote the disk velocity as $\frac{dr}{dt} = v_0$ and sphere velocity as $\frac{dR}{dt} = u_{\text{sphere}}$. Since $u_{\text{sphere}} = \frac{v}{\sqrt{R}}$, we have

$$v^2 = \frac{D}{3}v_0^2. \tag{A10}$$

For a disk $m = 0.5$, which with Eq. (12) we find a k value of

$$k = \frac{\pi D J v_0^2}{3}. \tag{A11}$$

This is precisely the same Avrami parameter from the classical treatment of a growing disk [33]. In this case, we find that v is the disk velocity v_0 scaled by a geometric constant. In general, this constant α can be defined as the scaling between v and v_0:

$$v = v_0/\alpha. \tag{A12}$$

It should be noted that v_0 is the true velocity of the growing crystal geometry, where v is the geometry-scaled velocity of the crystal.

APPENDIX B: CALCULATING THE CHANGE IN NUCLEATION AND GROWTH RATES RESULTING FROM A STEP CHANGE IN TEMPERATURE

What follows next will show how the difference in the solution before and after the temperature jump can be used to extract information about the change in growth velocity and nucleation rate. Recall that the transformed fraction is

$$f(t) = 1 - \exp\left(-\int_0^\infty \frac{4}{3}\pi r^3 \rho(r, t)\, dr\right). \tag{B1}$$

Now we will consider how the system solidifies shortly after the temperature jump. Since there has not been enough time for appreciable phase change due to the growth of newly nucleated solids after the temperature jump, then we can focus solely on the growth of the previously formed solids. Let us compare the time derivative of the transformed fraction slightly after the temperature to a case where the system remains at T_1 for all time to the case where we have a temperature jump from T_1 to T_2 at $t = s$. Since

$$\frac{\partial}{\partial t}(-\ln(1 - f(t))) = \frac{\partial}{\partial t}\int_0^\infty \frac{4}{3}\pi r^3 \rho(r, t) dr, \tag{B2}$$

given a velocity of $u_1(r)$, we know that at time $t = s$ we get a maximum phase inclusion radius $R_{\max}$ of:

$$R_{\max} = (v_1 s(m_1 + 1))^{\frac{1}{m_1+1}} \tag{B3}$$

Thus, we can ignore all values of $r > R_{\max}$. Next, by combining Eq. (17) from the main text and Eq. (B2), we have

$$\frac{\partial}{\partial t}(-\ln(1 - f(s))) = \frac{4}{3}\pi \int_0^{R_{\max}} r^3 \frac{\partial \rho_2(r, s)}{\partial t} dr. \tag{B4}$$

The following summarizes the solution for this integral. The phase size distribution after the temperature jump, its time derivative at the temperature jump, and corresponding time rate of phase change at the temperature jump are expressed as

$$\rho_2(r, t) = \frac{J_1}{v_1} r^{m_2} \theta(r^{m_2+1} - (m_2 + 1)v_2(t - s))$$
$$\times \theta\left(v_1 s - \frac{(r^{m_2+1} - (m_2 + 1)v_2(t - s))^{\frac{m_1+1}{m_2+1}}}{m_1 + 1}\right)$$
$$\times (r^{m_2+1} - (m_2 + 1)v_2(t - s))^{\frac{m_1-m_2}{m_2+1}}$$
$$+ \frac{J_2}{v_2} r^{m_2} \theta\left(v_2(t - s) - \frac{r^{m_2+1}}{m_2 + 1}\right), \tag{B5}$$

$$\frac{d\rho_2(r, s)}{dt} = v_2 \frac{J_1}{v_1}\left[\delta\left(sv_1 - \frac{r^{m_1+1}}{m_1 + 1}\right)r^{2m_1-m_2}\right.$$
$$\left. + \theta\left(sv_1 - \frac{r^{m_1+1}}{m_1 + 1}\right)(m_2 - m_1)r^{m_1-m_2-1}\right], \tag{B6}$$

$$\frac{\dot{f}_2(s)}{f_2(s) - 1} = \int_0^\infty \frac{4\pi}{3} r^3 \frac{\partial \rho(r, s)}{\partial t} dr, \tag{B7}$$

$$\frac{\dot{f}_2(s)}{f_2(s) - 1} = \frac{4\pi v_2}{3} \frac{J_1}{v_1} \int_0^\infty \delta\left(sv_1 - \frac{r^{m_1+1}}{m_1 + 1}\right)r^{3+2m_1-m_2}$$
$$+ \theta\left(sv_1 - \frac{r^{m_1+1}}{m_1 + 1}\right)(m_2 - m_1)r^{2+m_1-m_2} dr \tag{B8}$$

$$= \frac{\dot{f}_2(s)}{f_2(s) - 1} = I_1 + I_2. \tag{B9}$$

The first integral, I_1, is

$$I_1 = \frac{4\pi v_2}{3} \frac{J_1}{v_1} \int_0^\infty \delta\left(sv_1 - \frac{r^{m_1+1}}{m_1 + 1}\right)r^{3+2m_1-m_2} dr, \tag{B10}$$

$$y = sv_1 - \frac{r^{m_1+1}}{m_1 + 1}, \tag{B11}$$

$$r = ((v_1 s - y)(m_1 + 1))^{\frac{1}{m_1+1}}, \tag{B12}$$

$$dy = -r^{m_1}, \tag{B13}$$

$$I_1 = \frac{4\pi v_2}{3} \frac{J_1}{v_1} \int_0^{sv_1} \delta(y)((v_1 s - y)(m_1 + 1))^{\frac{3+m_1-m_2}{m_1+1}} dy, \tag{B14}$$

$$I_1 = \frac{4\pi v_2}{3} \frac{J_1}{v_1} R_{\max}^{3+m_1-m_2}. \tag{B15}$$

The second integral, I_2, is

$$I_2 = \frac{4\pi v_2}{3} \frac{J_1}{v_1} \int_0^\infty \theta\left(sv_1 - \frac{r^{m_1+1}}{m_1 + 1}\right)(m_2 - m_1)r^{2+m_1-m_2} dr, \tag{B16}$$

$$I_2 = \frac{4\pi v_2}{3} \frac{J_1}{v_1} \int_0^{R_{\max}} (m_2 - m_1)r^{2+m_1-m_2} dr. \tag{B17}$$

Taking the sum of I_1 and I_2, we get

$$\frac{\dot{f}_2(s)}{f_2(s) - 1} = \frac{4\pi v_2}{3} \frac{J_1}{v_1} R_{\max}^{3+m_1-m_2}\left[\frac{3}{3 + m_1 - m_2}\right]. \tag{B18}$$

We can substitute $m_1 = m_2$ and $v_1 = v_2$ to get $\dot{f}_1$ at $t = s$:

$$\frac{\dot{f}_1(s)}{f_1(s) - 1} = \frac{4\pi v_1}{3} \frac{J_1}{v_1} R_{\max}^3. \tag{B19}$$

Next, we can take the ratio of $\dot{f}_2$ and $\dot{f}_1$, noting that $f_1 = f_2$ at $t = s$:

$$\frac{\dot{f}_2(s)}{\dot{f}_1(s)} = \frac{v_2}{v_1} R_{\max}^{m_1-m_2}\left[\frac{3}{3 + m_1 - m_2}\right], \tag{B20}$$

$$\frac{\dot{f}_2(s)}{\dot{f}_1(s)} = \frac{v_2}{v_1} v_1^{\frac{m_1-m_2}{m_1+1}}(s(m_1 + 1))^{\frac{m_1-m_2}{m_1+1}}\left[\frac{3}{3 + m_1 - m_2}\right]. \tag{B21}$$

Thus, we arrive at

$$\frac{\dot{f}_2(s)}{\dot{f}_1(s)} = \beta \frac{v_2}{v_1^M}, \tag{B22}$$

$$\beta = (s(m_1 + 1))^{\frac{m_1-m_2}{m_1+1}}\left[\frac{3}{3 + m_1 - m_2}\right], \tag{B23}$$

$$M = \frac{m_2 + 1}{m_1 + 1}. \tag{B24}$$

1. Two-dimensional extension

Using the same reasoning as in three-dimensional case, we now consider circular, disk-equivalent growth in two-dimensions:

$$Ar^D = \pi R^2, \tag{B25}$$

$$r = \left(\frac{\pi}{A}R^2\right)^{\frac{1}{D}}, \tag{B26}$$

$$\alpha = \frac{2}{D}\left(\frac{\pi}{A}\right)^{\frac{1}{D}}, \tag{B27}$$

$$\frac{dr}{dt} = \alpha R^{\frac{2}{D}-1} \frac{dR}{dt}, \tag{B28}$$

$$m = \frac{2}{D} - 1, \tag{B29}$$

$$u(R) = \frac{v_0/\alpha}{R^m} = \frac{v}{R^m}. \tag{B30}$$

Following the same methods for deriving the three-dimensional case, we can derive the two-dimensional case for

the ratio of $\dot{f}_1$ and $\dot{f}_2$ at $t = s$:

$$\beta_{2D} = (s(m_1 + 1))^{\frac{m_1 - m_2}{m_1 + 1}} \left[\frac{2}{2 + m_1 - m_2} \right], \tag{B31}$$

$$M_{2D} = \frac{m_2 + 1}{m_1 + 1}, \tag{B32}$$

$$\frac{\dot{f}_2(s)}{\dot{f}_1(s)} = \beta_{2D} \frac{v_2}{v_1^{M_{2D}}}. \tag{B33}$$

Additionally, the two-dimensional Avrami parameters k and n can be rescaled from the three-dimensional version:

$$n = \frac{m + 3}{m + 1}, \tag{B34}$$

$$k = \pi \left(\frac{1 + m}{3 + m} \right) J((m + 1)v)^{\frac{2}{m+1}}. \tag{B35}$$

Thus, the two-dimensional nucleation rate equation is then

$$J(T) = \frac{k(T)n(T)}{\pi} \left[\frac{2v(T)}{n(T) - 1} \right]^{1 - n(T)}. \tag{B36}$$

APPENDIX C: TIME-DEPENDENT DIFFUSION LIMITED AGGREGATION PSEUDOCODE

The algorithms used in this work to generate diffusion limited aggregates and to then model time-dependent aggregate growth are summarized in Algorithm 1 and Algorithm 2, respectively.

Algorithm 1. Diffusion limited aggregation.

Input: $k, s, N, R_{\text{threshold}}$
Stickiness parameter, step size, number of particles, radius of gyration at temperature change
Output: p
Ordered array of aggregate particle locations

Choose initial seed location $p[0] = p_0$
for $n \leftarrow 1, N - 1$ **do**
    Calculate the minimum bounding circle S_{min} of p
    Calculate appearance and rejection circles S_r and S_a from S_{min}
    Chose a random point x on S_a
    while $x \notin p$ **do**
        Chose a random cardinal direction d
        $x \leftarrow x + sd$
        if x lies outside of S_r **then**
            Chose a random point y on S_a
            $x \leftarrow y$
        end if
        if x lies adjacent to any point in p **then**
            if rand $< k$ **then**
                $p[n] = x$
        end if
    end while
    Calculate the radius of gyration R_g
    if $R_g > R_{\text{threshold}}$ **then**
        Change s to alter the fractal dimension
    end if
end for

Algorithm 2. Time-dependent transformation and transformed fraction.

Input: $p, v, J_M, \Delta H_{\text{fus}}^{\circ}, M, N$
Ordered array of aggregate particle locations, DLA growth velocity, number of DLA nuclei formed per time step, heat of fusion, number of time steps, number of particles in p
Output: f, q, t
Transformed fraction, time, heat release

Calculate the radius of gyration $R_g[n]$ of the first n particles in p
Calculate $n_{\text{bin}} = \text{linspace}(0, N, M)$
for $m \leftarrow 0, M-$ **do**
    Calculate the radius of gyration $R[m] = R_g[n_{\text{bin}}[m]]$
end for
Calculate a and b from area vs radius of gyration $A = aR^b$
Using a, b, and A, calculate $t[m]$ such that $R[t] = vt$
Generate grid of zeros
for $m \leftarrow 0, M - 1$ **do**
    For J_M nuclei, place elements $n_{\text{bin}}[0]$ of p shifted by a random starting location on the grid. For existing aggregates, grow them by placing the next set of particles $n_{\text{bin}}[m_s]$ of p corresponding to m_s time steps since nucleation. Set the grid value to 1 every time a particle occupies a new unoccupied grid space. Apply periodic boundary conditions. Multiple p aggregates can be generated and sampled from for sufficient randomness.

    The transformed fraction $f[m]$ is the number of grid points equal to 1 divided by the total number of grid points. The heat release $q[m]$ is the number of new grid points added multiplied by the heat of fusion $\Delta H_{\text{fus}}^{\circ}$.
end for

[1] L. J. Lewis and R. M. Nieminen, Phys. Rev. B **54**, 1459 (1996).

[2] J. S. Poisson, J. P. Acker, J. G. Briard, J. E. Meyer, and R. N. Ben, Langmuir **35**, 7452 (2019).

[3] R. Strey, P. E. Wagner, and Y. Viisanen, J. Phys. Chem. **98**, 7748 (1994).

[4] G. C. Sosso, J. Chen, S. J. Cox, M. Fitzner, P. Pedevilla, A. Zen, and A. Michaelides, Chem. Rev. **116**, 7078 (2016).

[5] T. Li, D. Donadio, and G. Galli, Nat. Commun. **4**, 1 (2013).

[6] H. Laksmono, T. A. McQueen, J. A. Sellberg, N. D. Loh, C. Huang, D. Schlesinger, R. G. Sierra, C. Y. Hampton, D. Nordlund, M. Beye, A. V. Martin, A. Barty, M. M. Seibert, M. Messerschmidt, G. J. Williams, S. Boutet, K. Amann-Winkel, T. Loerting, L. G. M. Pettersson, M. J. Bogan *et al.*, J. Phys. Chem. Lett. **6**, 2826 (2015).

[7] S. A. Kulkarni, S. S. Kadam, H. Meekes, A. I. Stankiewicz, and J. H. ter Horst, Cryst. Growth Design **13**, 2435 (2013).

[8] S. Fan, X. Gu, X. Zhou, X. Duan, and H. Li, Energetic Mater. Front. **2**, 62 (2021).

[9] G. A. Kimmel, Y. Xu, A. Brumberg, N. G. Petrik, R. S. Smith, and B. D. Kay, J. Chem. Phys. **150**, 204509 (2019).

[10] S. Charoenrein and D. S. Reid, Thermochim. Acta **156**, 373 (1989).

[11] V. M. Fokin, A. A. Cabral, R. M. C. V. Reis, M. L. F. Nascimento, and E. D. Zanotto, J. Non-Cryst. Solids **356**, 358 (2010).

[12] E. Ma, C. V. Thompson, and L. A. Clevenger, J. Appl. Phys. **69**, 2211 (1991).

[13] K. F. Kelton, J. Am. Ceram. Soc. **75**, 2449 (1992).

[14] E. Aamir, Z. K. Nagy, and C. D. Rielly, Cryst. Growth Des. **10**, 4728 (2010).

[15] S. H. Neher, H. Klein, and W. F. Kuhs, J. Am. Ceram. Soc. **101**, 1381 (2018).

[16] V. M. Fokin, E. D. Zanotto, N. S. Yuritsyn, and J. W. Schmelzer, J. Non-Cryst. Solids **352**, 2681 (2006).

[17] D. W. Oxtoby, J. Phys.: Condens. Matter **4**, 7627 (1992).

[18] B. J. Murray, S. L. Broadley, T. W. Wilson, S. J. Bull, R. H. Wills, H. K. Christenson, and E. J. Murray, Phys. Chem. Chem. Phys. **12**, 10380 (2010).

[19] A. T. Lorenzo, M. L. Arnal, J. Albuerne, and A. J. Müller, Polymer Testing **26**, 222 (2007).

[20] M. Avrami, J. Chem. Phys. **7**, 1103 (1939).

[21] M. Avrami, J. Chem. Phys. **8**, 212 (1940).

[22] M. Avrami, J. Chem. Phys. **9**, 177 (1941).

[23] J. Málek, Thermochim. Acta **267**, 61 (1995).

[24] M. C. Weinberg, D. P. Birnie, and V. A. Shneidman, J. Non-Cryst. Solids **219**, 89 (1997).

[25] T. Matsui, T. Ogawa, and Y. Adachi, Results Mater. **1**, 100002 (2019).

[26] R. Saeki and T. Ohgai, Crystals **9**, 142 (2019).

[27] J. Yang, B. J. McCoy, and G. Madras, J. Phys. Chem. B **109**, 18550 (2005).

[28] J. Yang, B. J. McCoy, and G. Madras, J. Chem. Phys. **122**, 064901 (2005).

[29] J. R. Kangas, J. C. Bischof, and C. J. Hogan, J. Chem. Phys. **155**, 211101 (2021).

[30] B. Rheingans and E. J. Mittemeijer, JOM **65**, 1145 (2013).

[31] T. A. Witten and L. M. Sander, Phys. Rev. Lett. **47**, 1400 (1981).

[32] R. C. Ball and R. M. Brady, J. Phys. A: Math. Gen. **18**, L809 (1985).

[33] V. Hinrichs, G. Kalinka, and G. Hinrichsen, J. Macromol. Sci. Phys. **35**, 295 (1996).